JACS
JOURNAL OF THE AMERICAN CHEMICAL SOCIETY
Article
pubs.acs.org/JACS

Effect of Doping on the Magnetostructural Ordered Phase of Iron Arsenides: A Comparative Study of the Resistivity Anisotropy in Doped $BaFe_2As_2$ with Doping into Three Different Sites

Shigeyuki Ishida,*[,†,‡,§] Masamichi Nakajima,[†,‡,§] Tian Liang,[†,‡,§] Kunihiro Kihou,[‡,§] Chul-Ho Lee,[‡,§] Akira Iyo,[‡,§] Hiroshi Eisaki,[‡,§] Teruhisa Kakeshita,[†,§] Yasuhide Tomioka,[‡,§] Toshimitsu Ito,[‡,§] and Shin-ichi Uchida[†,§]

[†]Department of Physics, University of Tokyo, Tokyo 113-0033, Japan
[‡]National Institute of Advanced Industrial Science and Technology, Tsukuba 305-8568, Japan
[§]Transformative Research Project on Iron Pnictides, Japan Science and Technology Agency (JST), Tokyo 102-0075, Japan

ABSTRACT: To unravel the role of doping in iron-based superconductors, we investigated the in-plane resistivity of $BaFe_2As_2$ doped at one of the three different lattice sites, $Ba(Fe_{1-x}Co_x)_2As_2$, $BaFe_2(As_{1-x}P_x)_2$, and $Ba_{1-x}K_xFe_2As_2$, focusing on the doping effect in the low-temperature antiferromagnetic/orthorhombic (AFO) phase. A major role of doping in the high-temperature paramagnetic/tetragonal (PT) phase is known to change the Fermi surface by supplying charge carriers or exerting chemical pressure. In the AFO phase, we found a clear correlation between the magnitude of the residual resistivity and the resistivity anisotropy. This indicates that the resistivity anisotropy originates from anisotropic impurity scattering due to dopant atoms. The magnitude of the residual resistivity was also found to be a parameter controlling the suppression rate of the AFO ordering temperature. Therefore, the dominant role of doping in the AFO phase is to introduce disorder to the system, distinct from that in the PT phase.

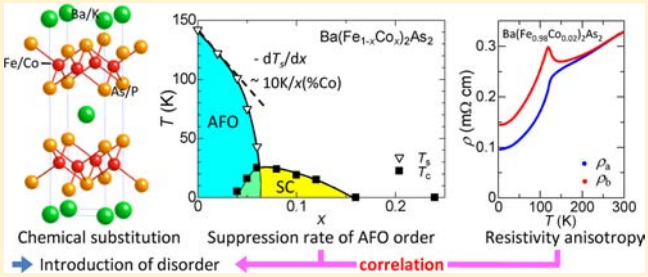

INTRODUCTION

The iron arsenides, which are in most cases antiferromagnetic (AF) metals with orthorhombic lattice distortions in their parent phase, can be turned into high-transition-temperature (high-T_c) superconductors by chemical substitution/doping.[1−4] The temperature−doping (T−x) phase diagram of iron pnictides is similar to that of high-T_c cuprates in that the system moves from an AF phase to a superconducting (SC) phase as the doping level increases. As in the case of the high-T_c cuprates, it is worth investigating the evolution of the electronic state with doping in order to understand the real nature of the AF metallic state and how it is linked to the SC phase.

One notable feature of the antiferromagnetic/orthorhombic (AFO) phase of iron-based superconductors is an anisotropic electronic state. In the AFO phase of iron arsenides, the anisotropic electronic state has been revealed by neutron scattering,[5] transport,[6] and optical measurements[7] and by angle-resolved photoemission spectroscopy (ARPES)[8] and scanning tunneling spectroscopy (STS).[9] Except for the resistivity anisotropy, the origin of the anisotropy in these spectra is inherent to the electronic state of the AFO phase, which is characterized by stripe-AF spin order and orthorhombic lattice distortions, possibly connected to orbital ordering/polarization. Extensive theoretical and experimental efforts have been devoted to understanding its origin.

Identification of the roles played by chemical doping is another important issue. In the case of high-T_c cuprates, a crucial role of doping is to tune the carrier concentration and in some cases to introduce disorder.[10,11] In an analogous way, for example, substitution of Co (K) for Fe (Ba) in $BaFe_2As_2$ chemically works as electron (hole) doping, which is also supported by the evolution of the volume of the Fermi surface (FS) as observed by ARPES.[12,13] On the other hand, the phase diagram of $BaFe_2As_2$ with P substituted for As, which does not change the carrier concentration (dubbed as isovalent doping), is similar to that in other doping cases.[4] This suggests that changing the carrier concentration is not the only effect of doping.

To date, the evolution of physical properties with doping has been investigated for one particular system. However, to achieve a unified view of the phase diagram of iron-based superconductors, a comprehensive study to investigate the similarities and differences among various doping routes leading toward the superconducting phase is necessary. In this work, we focused on the AFO phase of the representative iron arsenide $BaFe_2As_2$ and investigated the effects of Co, P, and K doping by studying the doping evolution of the in-plane resistivity and its anisotropy. We found that in all the three cases the major role

Received: November 14, 2012
Published: January 23, 2013

   dx.doi.org/10.1021/ja311174e | J. Am. Chem. Soc. 2013, 135, 3158−3163

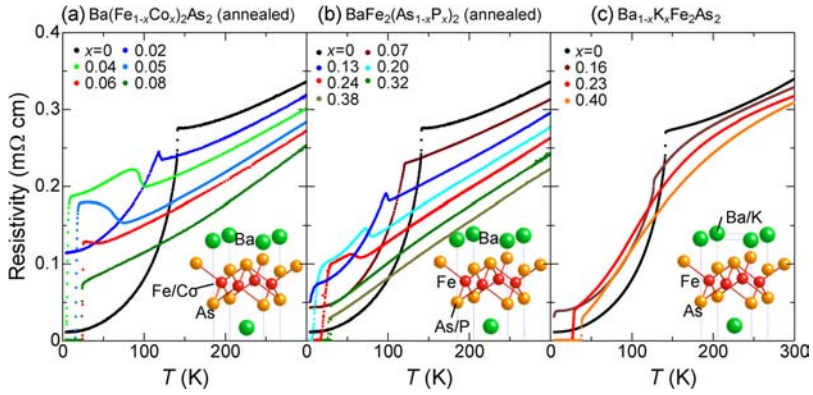

Figure 1. Doping evolution of the temperature dependence of the in-plane resistivity for (a) $Ba(Fe_{1-x}Co_x)_2As_2$, (b) $BaFe_2(As_{1-x}P_x)_2$, and (c) $Ba_{1-x}K_xFe_2As_2$ in the underdoped regime.

of doping is to introduce disorder, the effect of which is strongly dependent on the dopant site. We show that strength of the scattering from dopant atoms controls the suppression rate of the AFO phase as well as the resistivity anisotropy.

RESULTS AND DISCUSSION

Doping Evolution of the In-Plane Resistivity in the AFO Phase. Figure 1 shows the temperature dependences of the in-plane resistivity for $Ba(Fe_{1-x}Co_x)_2As_2$, $BaFe_2(As_{1-x}P_x)_2$, and $Ba_{1-x}K_xFe_2As_2$, covering the doping range from $x = 0$ to the composition just above the AFO−SC coexistence region. The resistivity of the parent $BaFe_2As_2$ exhibits an abrupt decrease below $T_s = 143$ K associated with the transition from the paramagnetic/tetragonal (PT) phase to the AFO phase. The decrease in the resistivity despite the loss of carrier density is due to a reconstruction of the Fermi surface in the AFO phase that generates high-mobility carriers, which dominate the charge transport.[14,15] The residual resistivity is quite low ($\rho_0 \approx 10\ \mu\Omega$ cm) for a well-annealed high-quality crystal.

When Co is substituted for Fe, the residual resistivity in the AFO phase rapidly increases up to $x = 0.04$ (Figure 2a), which indicates that the Co atom works as a strong scattering center. For $x = 0.02$, $\rho_0/x \approx 60\ \mu\Omega$ cm/x(%Co), which is comparable with the residual resistivity produced by a Zn impurity introduced into underdoped cuprates.[10] With further doping, however, the residual resistivity starts to decrease, accompanied by the appearance of superconductivity. A drop in the scattering rate was observed in the IR spectrum for $Ba(Fe_{1-x}Co_x)_2As_2$ for $x > 0.04$.[16] This result suggests the formation of unusual impurity states around a Co atom in the AFO phase.

In the case of $BaFe_2(As_{1-x}P_x)_2$, the doping evolution of the resistivity is qualitatively similar to that of $Ba(Fe_{1-x}Co_x)_2As_2$. However, the magnitude of the residual resistivity (Figure 2b) is smaller than that of $Ba(Fe_{1-x}Co_x)_2As_2$ by an order of magnitude, indicating that a P atom substituted for As scatters carriers less strongly than a Co substituted for Fe. The isovalency of P to As is probably responsible for the weaker scattering.

The doping evolution of the in-plane resistivity of $Ba_{1-x}K_xFe_2As_2$ is entirely different from that observed in the above two cases. The residual resistivity is smaller by an order of magnitude. In view of the fact that annealing is difficult for $Ba_{1-x}K_xFe_2As_2$ crystals and as-grown crystals therefore likely contain crystal disorder/deficiency near the FeAs block, the K-induced residual resistivity of $Ba_{1-x}K_xFe_2As_2$ would be

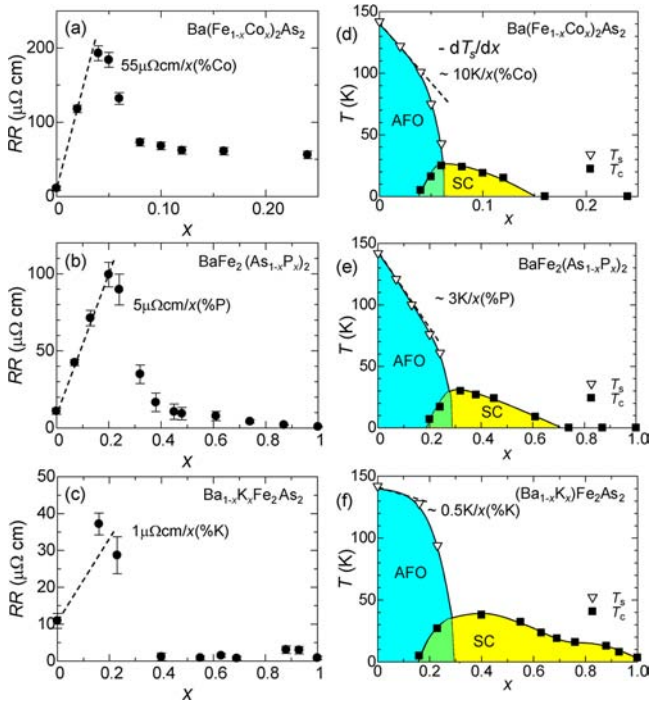

Figure 2. Doping dependence of the residual resistivity of (a) $Ba(Fe_{1-x}Co_x)_2As_2$, (b) $BaFe_2(As_{1-x}P_x)_2$, and (c) $Ba_{1-x}K_xFe_2As_2$. Dashed lines indicate the increases in residual resistivity upon doping, and the increasing rates (indicated by the slopes) are also shown. (d−f) Phase diagrams for the three compounds based on the in-plane resistivity measurements. Also shown are the suppression rates of AFO ordering ($-dT_s/dx$).

practically zero over the whole doping range. Therefore, the magnitude of the residual resistivity, or the strength of the impurity scattering by dopant atoms, gets smaller as the dopant site moves farther away from the Fe plane. It should be noted that the scattering strength of an individual dopant atom shows an overall decrease with increasing dopant concentration, which is certainly associated with weakening of the AFO order.[17] Below, we show that the strength of the impurity scattering is intimately related to the magnitude of the resistivity anisotropy as well as the suppression rate of the AFO order.

Suppression of the AFO Phase by Chemical Substitution. In the case of cuprates, the AF order is rapidly destroyed by doping a small fraction of holes (~2%)[18] but it is robust toward Zn substitution for Cu and persists at Zn

dx.doi.org/10.1021/ja311174e | J. Am. Chem. Soc. 2013, 135, 3158−3163

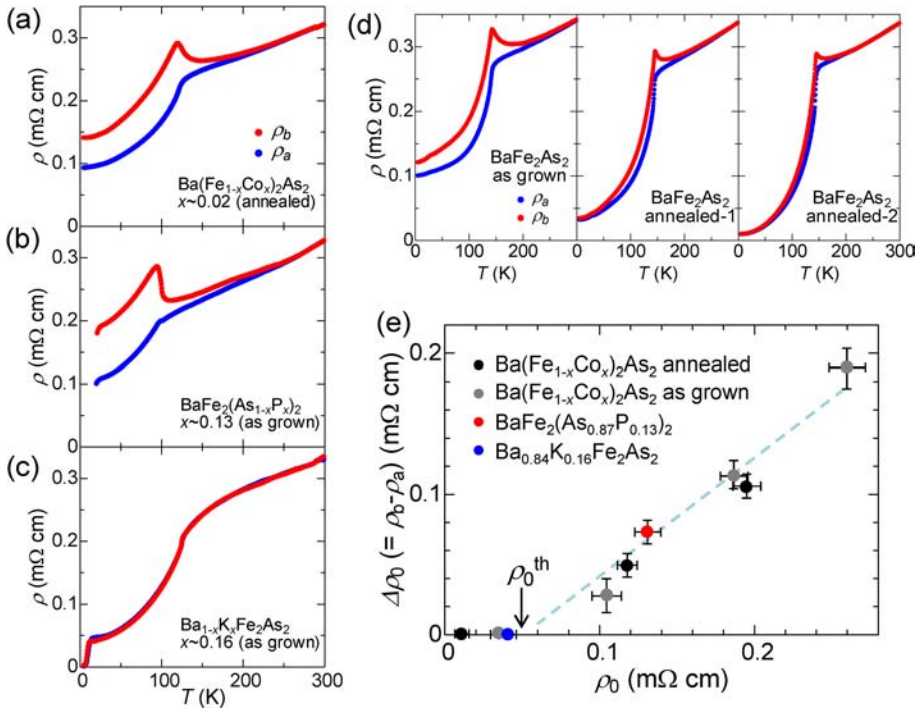

Figure 3. (a–d) In-plane resistivity anisotropies of selected compounds: (a) annealed $Ba(Fe_{0.98}Co_{0.02})_2As_2$; (b) as-grown $BaFe_2(As_{0.87}P_{0.13})_2$; (c) as-grown $Ba_{0.84}K_{0.16}Fe_2As_2$; (d) as-grown and annealed $BaFe_2As_2$. The annealing times were different for the annealed-1 (shorter) and annealed-2 (longer) $BaFe_2As_2$ samples in (d). (e) Difference in the residual component of the in-plane resistivity ($\Delta\rho_0 = \rho_b - \rho_a$) at low temperature as a function of the residual resistivity. ρ_0^{th} indicates the threshold value of the residual resistivity at which the resistivity anisotropy appears.

concentrations as large as 25%.[19] These experimental results can be reproduced by the magnetic frustration and magnetic dilution models for a two-dimensional Heisenberg antiferromagnet,[20] respectively. We investigated the suppression rate of the AFO order ($-dT_s/dx$) for the three kinds of doping into $BaFe_2As_2$.

In the case of Co doping, the AFO phase is radically suppressed at a rate of $(-dT_s/dx) \approx 10$ K/x(%Co) below $x = 0.05$ (Figure 2d). With further doping ($x \geq 0.05$), superconductivity appears and the decrease in T_s speeds up. If one assumes that each Co atom introduces one mobile electron (although there is controversy about whether the substituted Co atoms supply carriers[21−23]), it seems to frustrate the Fe spin order.

The isovalent P substitution neither introduces charge carriers nor dilutes the Fe spins, so the effect of P substitution on the AF spin order is expected to be very weak. However, as in the case of Co doping, P doping reduces T_s at a rate of $(-dT_s/dx) \approx 3$ K/x(%P) for $x < 0.2$, about one-third of that for Co doping (Figure 2e). The case of K doping is unusual. Substitution of a K atom for a Ba atom adds one hole to the AF order state, but the suppression rate of T_s is very small, at least in the low-doping region (Figure 2f). We obtained only three data points in the underdoped regime, but the data in refs 24 and 25 confirm that the suppression of T_s is very slow, with $(-dT_s/dx) < 0.5$ K/x(%K) up to $x < 0.15$, although T_s starts to decrease rapidly once the SC phase appears ($x > 0.15$) and coexists with the AFO phase.

These results for the three types of doping show that the mechanism of suppression of the AFO phase with doping in $BaFe_2As_2$ is quite different from that of the localized spin AF order in cuprates. Interestingly, we notice that for the three types of doping, the suppression rate of the AFO phase decreases in the order of decreasing residual resistivity produced by doping. This suggests that a disorder effect plays a substantial role in the suppression of the AFO phase. On the basis of itinerant magnetism [spin density wave (SDW)], Vavilov and Chubukov explained a linear suppression of T_s (T_N) as a disorder/impurity effect with the suppression rate being determined by the carrier scattering rate,[26] in apparent agreement with the present results. In fact, the T_s suppression rate is also very small in the 1111 systems $LnFeAsO_{1-x}F_x$ and $LnFeAsO_{1-y}$ (Ln = rare-earth element),[27,28] where the dopant atoms or vacancies are located at the O site far away from the FeAs block.

At this point, the possibility that a change in the lattice parameters with doping is another driving force for suppressing the AFO order should also be considered. It is known that the AFO order is also suppressed by the application of hydrostatic pressure.[29] For P doping, the lattice constants shrink appreciably in both the a and c directions, so the reduction in volume is most remarkable.[30] The relatively rapid decrease in T_s in the P-doping case despite the fact that the residual resistivity is a factor of ∼10 smaller than that of the Co-doped compound indicates that the chemical pressure effect is also at work in suppressing the AFO order. Since the volume reduction rate is smaller for Co doping[31] and much smaller for K doping,[32] the chemical pressure effect is not expected to be significant in those two cases.

We see that in all the three cases, T_s rapidly decreases once the SC phase appears and coexists with the AFO order. A naive explanation for this is that the AFO−PT/SC transition is essentially first order, and hence, T_s should have exhibited a discontinuous decrease at the transition. In this context, a small spatial fluctuation of the dopant concentration would lead to coexistence/phase separation of the two phases and make T_s

dx.doi.org/10.1021/ja311174e | J. Am. Chem. Soc. 2013, 135, 3158−3163

decrease continuously but rapidly. As supportive evidence, in the case of application of pressure, which is a cleaner control parameter than chemical doping, and in the doped 1111 system, where the effect of dopant disorder is weakest, T_s decreased sharply and there was almost no AFO−SC coexistence region.[29]

It should be noted that a major effect of these chemical dopings in the PT phase is to change the Fermi surface by adding extra electrons or holes or by exerting chemical pressure.[13,33,34] A disorder effect due to dopant impurities may be seen in the superconducting dome (T_c−x curve). The maximum value of T_c and the width of the dome decrease in the order of K, P, and Co doping (Figure 2d−f), which is just the order of increasing disorder strength observed in the AFO phase.

Origin of the In-Plane Resistivity Anisotropy. Originally, the resistivity anisotropy was considered to arise directly from the intrinsically anisotropic electronic state of the AFO phase. For the Co-doped system, the resistivity along the shorter b axis with ferromagnetic spin alignment (ρ_b) is always higher than that along the longer a axis with antiferromagnetic spin alignment (ρ_a). This looks odd in view of, for example, the double-exchange mechanism but is in agreement with the anisotropy in the low-energy optical conductivity ($\sigma_a > \sigma_b$).[7] The anisotropy in optical conductivity is explained by theories that take into account stripe-AF spin order and/or orbital correlations (ordering).[35]

In the preceding work,[36] we investigated the anisotropy of the in-plane resistivity in the AFO phase of underdoped $Ba(Fe_{1-x}Co_x)_2As_2$. We found that (1) the resistivity anisotropy at low temperatures almost vanishes for clean $BaFe_2As_2$, (2) a finite anisotropy is induced by Co doping in the residual resistivity component, and (3) the anisotropy in as-grown crystals probably arises from crystal defects present in nearby FeAs blocks. These findings evidenced that the resistivity anisotropy originates from the anisotropic impurity scattering by doped Co atoms/crystal defects. A Co impurity atom introduced into the AFO phase is supposed to polarize its electronic surroundings with intrinsic anisotropy, thereby working as an anisotropic scattering center. The impurity-induced resistivity anisotropy scenario is supported by optical measurements performed on detwinned $Ba(Fe_{1-x}Co_x)_2As_2$.[17] The width of the Drude component, which is proportional to the carrier scattering rate $1/\tau$, was found to increase in proportion to the Co concentration and become larger along the b axis than along the a axis. Moreover, recent STS measurements discovered the formation of a-axis-aligned electronic dimers surrounding each Co in the AFO state of $Ca(Fe_{1-x}Co_x)_2As_2$,[37] in agreement with our speculation of the anisotropic Co impurity state.

Here we extended the measurements to P- and K-doped compounds. Figure 3b,c shows the in-plane resistivity anisotropies of $BaFe_2(As_{1-x}P_x)_2$ ($x \approx 0.13$) and $Ba_{1-x}K_xFe_2As_2$ ($x \approx 0.16$), respectively, and the results for $Ba(Fe_{1-x}Co_x)_2As_2$ ($x = 0.02$), which has similar values of T_s, are also shown (Figure 3a). Unfortunately, the measurements on the P- and K-doped compounds were performed on as-grown crystals. Damaged or contaminated surface layers of annealed crystals should be removed in order to obtain reliable data. However, since the as-grown P- and K-doped crystals were thinner than the Co-doped one, the crystals became too thin for application of uniaxial pressure after the damaged surface layers were removed.

$BaFe_2(As_{1-x}P_x)_2$ was found to show a sizable resistivity anisotropy as well. As in the case of $Ba(Fe_{1-x}Co_x)_2As_2$, the resistivity along the b axis was higher than that along the a axis. However, in view of the fact that the dopant concentration x was larger for the P-doped case, the magnitude of the anisotropy was smaller. Thus, it is likely that a doped P atom forms a similar anisotropic impurity state and acts as an anisotropic scattering center with a smaller scattering cross section than for a Co impurity.

By contrast, $Ba_{1-x}K_xFe_2As_2$ did not show a discernible anisotropy (Figure 3c), in agreement with the previous report.[38] It was argued that resistivity anisotropy is a property inherent to electron-doped compounds. However, the presence of anisotropy in the isovalent P-doped compound calls this hypothesis into question.

The absence of resistivity anisotropy seems odd in view of the results for Co and P doping, as a sizable residual resistivity (30−40 $\mu\Omega$ cm) was observed for the K-doped compound. However, when collecting the in-plane resistivity anisotropy data for various samples, including as-grown $Ba(Fe_{1-x}Co_x)_2As_2$, we found a correlation between the magnitude of the resistivity anisotropy, $\Delta\rho_0 = \rho_b - \rho_a$, and the residual resistivity ρ_0 measured for the free-standing (twinned) crystal, which coincides with the average residual resistivity $(\rho_a + \rho_b)/2$ (Figure 3e). Since the magnitude of ρ_0 is a measure of the impurity scattering rate, this correlation confirms again our conclusion that the resistivity anisotropy originates from impurity scattering, irrespective of the sign of the introduced charge carrier (electron or hole). Furthermore, there appeared to be a threshold value of the residual resistivity ($\rho_0^{th} \approx 50$ $\mu\Omega$ cm) above which finite $\Delta\rho_0$ appeared. This suggests that when the impurity potential is too weak, the unusual anisotropic impurity state is not formed, as might be the case with K doping and the annealed parent compound.

As we demonstrated previously,[14,44] both residual resistivity and resistivity anisotropy decrease after annealing. Particularly for $BaFe_2As_2$, sufficient annealing makes the resistivity anisotropy vanishingly small at low temperatures (Figure 3d). This in turn implies that the as-grown crystal might contain defects and impurities in nearby FeAs blocks that also can act as anisotropic scattering centers. Thus, the resistivity anisotropy of the as-grown $BaFe_2(As_{1-x}P_x)_2$ crystal might be induced by both P atoms and crystal defects. To estimate the genuine resistivity anisotropy induced by P atoms, we compared the magnitudes of ρ_0 for as-grown and annealed $BaFe_2(As_{1-x}P_x)_2$ ($x \approx 0.13$). The value of ρ_0 was ∼130 $\mu\Omega$ cm for the as-grown crystal, which was reduced to 80 $\mu\Omega$ cm after annealing. Annealing would be expected to reduce the defect density considerably, so ρ_0 for the annealed crystal should be attributable for the most part to the contribution from the P impurity. Since this value is well above the threshold value ρ_0^{th}, the P impurity likely induces the residual resistivity. From the correlation between ρ_0 and $\Delta\rho$ displayed in Figure 3e, the magnitude of $\Delta\rho$ induced by the P impurity would be 20−40 $\mu\Omega$ cm.

As-grown $Ba_{1-x}K_xFe_2As_2$ is also expected to contain crystal defects. However, in view of the small value of ρ_0 for the x = 0.16 crystal (∼37 $\mu\Omega$ cm), which is below ρ_0^{th}, the contribution to $\Delta\rho_0$ from the crystal defects is negligibly small. The formation of crystal defects is probably inhibited under the conditions for the crystal growth of K-doped compounds. Therefore, it is reasonable to conclude that the K impurity potential is too weak to induce resistivity anisotropy. The possibility that the anisotropy induced by crystal defects

dx.doi.org/10.1021/ja311174e | J. Am. Chem. Soc. 2013, 135, 3158−3163

accidentally compensates for that due to the K impurity with opposite sign has been ruled out.[39,40]

We have shown that the anisotropic elastic scattering from dopant impurities is responsible for the resistivity anisotropy at low temperatures in the AFO phase. However, as displayed in Figure 4, the anisotropy $\Delta\rho = \rho_b - \rho_a$ gradually increases as the temperature is raised toward T_s. Above T_s, $\Delta\rho$ drops sharply after showing a cusp at T_s but remains finite at temperatures well above T_s. As the temperature rises, inelastic scattering processes progressively dominate. Therefore, the enhanced anisotropy at high temperatures is indicative of the presence of an anisotropic contribution to the inelastic scattering process. According to Fernandes et al.,[39] this gives rise to the resistivity anisotropy combined with impurity scattering. This mechanism might explain the enhanced anisotropy at elevated temperatures below T_s as well as the anisotropy above T_s. The anisotropy above T_s (in the tetragonal phase) is usually attributed to a manifestation of the rotational-symmetry-broken nematic phase.[6] However, because the resistivity anisotropy arises predominantly from impurity scattering and the temperature range of the anisotropy above T_s expands with Co/P doping and shrinks after annealing, it would be possible to suppose that an extrinsic mechanism is also at work, such as short-range AFO order locally induced around impurity atoms.

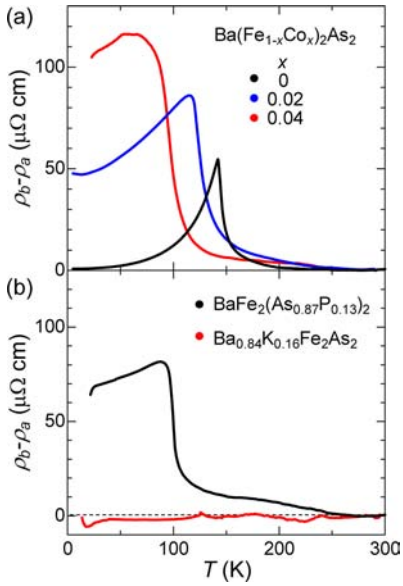

Figure 4. Resistivity anisotropy $\Delta\rho = \rho_b - \rho_a$ plotted as a function of temperature for (a) $Ba(Fe_{1-x}Co_x)_2As_2$ with $x = 0$, 0.02, and 0.04 and (b) $BaFe_2(As_{1-x}P_x)_2$ with $x = 0.13$ and $Ba_{1-x}K_xFe_2As_2$ with $x = 0.16$.

CONCLUSIONS

We have investigated the doping evolution and dopant-site dependence of the in-plane resistivity for $BaFe_2As_2$ to pursue the effect of doping on the AFO phase. The strength of the dopant impurity scattering was found to be a control parameter for the suppression of the AFO ordering temperature, in addition to the chemical pressure exerted by substituted dopant atoms. It also controls the magnitude of the resistivity anisotropy, which arises from an anomalous impurity state formed around a dopant atom. The anisotropy diminishes when the dopant site is away from the Fe plane and the impurity potential is too weak to form such an impurity state. Therefore, the major effect of doping on the AFO phase is to introduce disorder. Formation of the anomalous impurity state around a dopant atom is a hallmark of a unique electronic state of the AFO phase that might be regarded as a spin-charge-orbital complex. The fact that the superconducting transition temperature T_c attains maximum values near the AFO−SC phase boundary suggests that fluctuations of such a complex may be relevant to the formation of Cooper pairs in doped iron arsenides.

EXPERIMENTAL SECTION

Single crystals of $Ba(Fe_{1-x}Co_x)_2As_2$, $BaFe_2(As_{1-x}P_x)_2$, and $Ba_{1-x}K_xFe_2As_2$ were grown by the self-flux method.[16,41,42] The actual compositions of the samples were determined by inductively coupled plasma and energy-dispersive X-ray analyses. The crystals were cut in a rectangular shape along the tetragonal [110] directions, which become *a* or *b* axes in the orthorhombic phase. Typical dimensions of the $Ba(Fe_{1-x}Co_x)_2As_2$ crystals were 1.5 mm × 1.5 mm in the *ab* plane and 0.5 mm in thickness along the *c* axis. In the case of $BaFe_2(As_{1-x}P_x)_2$ and $Ba_{1-x}K_xFe_2As_2$, the crystals were thinner (0.1−0.2 mm in thickness). The crystals of Co- and P-doped $BaFe_2As_2$ were sealed into an evacuated quartz tube together with BaAs powder and annealed for several days, since annealing remarkably improves the transport properties in the ordered phase of $BaFe_2As_2$,[43] indicating that the as-grown crystals contain appreciable amount of defects/impurities that might inhibit the observation of the intrinsic charge transport in this system. However, for K-doped $BaFe_2As_2$, annealing damaged the crystals, so the measurements were done on as-grown crystals. For detwinning, the rectangular-shaped crystals were set in an uniaxial pressure cell and detwinned by the application of compressive pressure along the tetragonal (110) direction.[44] The resistivities along the *a* and *b* axes were measured simultaneously using the Montgomery method[45] without releasing the pressure. The measurements were performed using a Quantum Design Physical Property Measurement System (PPMS).

AUTHOR INFORMATION

Corresponding Author

s.ishida@aist.go.jp

Notes

The authors declare no competing financial interest.

ACKNOWLEDGMENTS

S.I. and M.N. thank the Japan Society for the Promotion of Science (JSPS) for financial support. This work was supported by the Transformative Research Project on Iron Pnictides (TRIP) from the Japan Science and Technology Agency, the Japan−China−Korea A3 Foresight Program from JSPS, and a Grant-in-Aid for Scientific Research from the Ministry of Education, Culture, Sports, Science, and Technology of Japan.

REFERENCES

(1) Kamihara, Y.; Watanabe, T.; Hirano, M.; Hosono, H. *J. Am. Chem. Soc.* **2008**, *130*, 3296.
(2) Rotter, M.; Tegel, M.; Johrendt, D. *Phys. Rev. Lett.* **2008**, *101*, No. 107006.
(3) Sefat, A. S.; Jin, R.; McGuire, M. A.; Sales, B. C.; Singh, D. J.; Mandrus, D. *Phys. Rev. Lett.* **2008**, *101*, No. 117004.
(4) Jiang, S.; Xing, H.; Xuan, G.; Wang, C.; Ren, Z.; Feng, C.; Dai, J.; Xu, Z.; Cao, G. *J. Phys.: Condens. Matter* **2009**, *21*, No. 382203.
(5) Zhao, J.; Adroja, D. T.; Yao, D.-X.; Bewley, R.; Li, S.; Wang, X. F.; Wu, G.; Chen, X. H.; Hu, J.; Dai, P. *Nat. Phys.* **2009**, *5*, 555.
(6) Chu, J.-H.; Analytis, J. G.; De Greve, K.; McMahon, P. L.; Islam, Z.; Yamamoto, Y.; Fisher, I. R. *Science* **2010**, *329*, 824.

(7) Nakajima, M.; Liang, T.; Ishida, S.; Tomioka, Y.; Kihou, K.; Lee, C. H.; Iyo, A.; Eisaki, H.; Kakeshita, T.; Ito, T.; Uchida, S. *Proc. Natl. Acad. Sci. U.S.A.* **2011**, *108*, 12238.
(8) Yi, M.; Lu, D. H.; Chu, J.-H.; Analytis, J. G.; Sorini, A. P.; Kemper, A. F.; Moritz, B.; Mo, S.-K.; Moore, R. G.; Hashimoto, M.; Lee, W. S.; Hussain, Z.; Devereaux, T. P.; Fisher, I. R.; Shen, Z.-X. *Proc. Natl. Acad. Sci. U.S.A.* **2011**, *108*, 6878.
(9) Chuang, T.-M.; Allan, M. P.; Lee, J.; Xie, Y.; Ni, N.; Bud'ko, S. L.; Boebinger, G. S.; Canfield, P. C.; Davis, J. C. *Science* **2010**, *327*, 181.
(10) Fukuzumi, Y.; Mizuhashi, K.; Takenaka, K.; Uchida, S. *Phys. Rev. Lett.* **1996**, *76*, 684.
(11) Eisaki, H.; Kaneko, N.; Feng, D. L.; Damascelli, A.; Mang, P. K.; Shen, K. M.; Shen, Z.-X.; Greven, M. *Phys. Rev. B* **2004**, *69*, No. 064812.
(12) Liu, C.; Kondo, T.; Fernandes, R. M.; Palczewski, A. D.; Mun, E. D.; Ni, N.; Thaler, A. N.; Bostwick, A.; Rotenberg, E.; Schmalian, J.; Bud'ko, S. L.; Canfield, P. C.; Kaminski, A. *Nat. Phys.* **2010**, *6*, 419.
(13) Malaeb, W.; Shimojima, T.; Ishida, Y.; Okazaki, K.; Ota, Y.; Ohgushi, K.; Kihou, K.; Saito, T.; Lee, C. H.; Ishida, S.; Nakajima, M.; Uchida, S.; Fukazawa, H.; Kohori, Y.; Iyo, A.; Eisaki, H.; Chen, C.-T.; Watanabe, S.; Ikeda, H.; Shin, S. *Phys. Rev. B* **2012**, *86*, 165117.
(14) Ishida, S.; Liang, T.; Nakajima, M.; Kihou, K.; Lee, C. H.; Iyo, A.; Eisaki, H.; Kakeshita, T.; Kida, T.; Hagiwara, M.; Tomioka, Y.; Ito, T.; Uchida, S. *Phys. Rev. B* **2011**, *84*, No. 184514.
(15) Terashima, T.; Kurita, N.; Tomita, M.; Kihou, K.; Lee, C. H.; Tomioka, Y.; Ito, T.; Iyo, A.; Eisaki, H.; Liang, T.; Nakajima, M.; Ishida, S.; Uchida, S.; Harima, H.; Uji, S. *Phys. Rev. Lett.* **2011**, *107*, No. 176402.
(16) Nakajima, M.; Ishida, S.; Kihou, K.; Tomioka, Y.; Ito, T.; Yoshida, Y.; Lee, C. H.; Kito, H.; Iyo, A.; Eisaki, H.; Kojima, K. M.; Uchida, S. *Phys. Rev. B* **2010**, *81*, No. 104528.
(17) Nakajima, M.; Ishida, S.; Tomioka, Y.; Kihou, K.; Lee, C. H.; Iyo, A.; Ito, T.; Kakeshita, T.; Eisaki, H.; Uchida, S. *Phys. Rev. Lett.* **2012**, *109*, No. 217003.
(18) Keimer, B.; Belk, N.; Birgeneau, R. J.; Cassanho, A.; Chen, C. Y.; Greven, M.; Kastner, M. A.; Aharony, A.; Endoh, Y.; Erwin, R. W.; Shirane, G. *Phys. Rev. B* **1992**, *46*, 14034.
(19) Hücker, M.; Kataev, V.; Pommer, J.; Harrass, J.; Hosni, A.; Pflitsch, C.; Gross, R.; Büchner, B. *Phys. Rev. B* **1999**, *59*, R725.
(20) Korenblit, I. Y.; Aharony, A.; Entin-Wohlman, O. *Phys. Rev. B* **1999**, *60*, R15017.
(21) Levy, G.; Sutarto, R.; Chevrier, D.; Regier, T.; Blyth, R.; Geck, J.; Wurmehl, S.; Harnagea, L.; Wadati, H.; Mizokawa, T.; Elfimov, I. S.; Damascelli, A.; Sawatzky, G. A. *Phys. Rev. Lett.* **2012**, *109*, No. 077001.
(22) Wadati, H.; Elfimov, I.; Sawatzky, G. A. *Phys. Rev. Lett.* **2010**, *105*, No. 157004.
(23) Kemper, A. F.; Cao, C.; Hirschfeld, P. J.; Cheng, H.-P. *Phys. Rev. B* **2009**, *80*, No. 104511.
(24) Avci, S.; Chmaissem, O.; Chung, D. Y.; Rosenkranz, S.; Goremychkin, E. A.; Castellan, J.-P.; Todorov, I. S.; Schlueter, J. A.; Claus, H.; Daoud-Aladine, A.; Khalyavin, D. D.; Kanatzidis, M. G.; Osborn, R. *Phys. Rev. B* **2012**, *85*, No. 184507.
(25) Ohgushi, K.; Kiuchi, Y. *Phys. Rev. B* **2012**, *85*, No. 064522.
(26) Vavilov, M. G.; Chubukov, A. V. *Phys. Rev. B* **2011**, *84*, No. 214521.
(27) Luetkens, H.; Klauss, H.-H.; Kraken, M.; Litterst, F. J.; Dellmann, T.; Klingeler, R.; Hess, C.; Khasanov, R.; Amato, A.; Baines, C.; Kosmala, M.; Schumann, O. J.; Braden, M.; Hamann-Borrero, J.; Leps, N.; Kondrat, A.; Behr, G.; Werner, J.; Büchner, B. *Nat. Mater.* **2009**, *8*, 305.
(28) Hess, C.; Kondrat, A.; Narduzzo, A.; Hamann-Borrero, J. E.; Klingeler, R.; Werner, J.; Behr, G.; Büchner, B. *EPL* **2009**, *87*, No. 17005.
(29) Colombier, E.; Bud'ko, S. L.; Ni, N.; Canfield, P. C. *Phys. Rev. B* **2009**, *79*, No. 224518.
(30) Kasahara, S.; Shibauchi, T.; Hashimoto, K.; Ikada, K.; Tonegawa, S.; Okazaki, R.; Ikeda, H.; Takeya, H.; Hirata, K.; Terashima, T.; Matsuda, Y. *Phys. Rev. B* **2010**, *81*, No. 184519.
(31) Ni, N.; Tillman, M. E.; Yan, J.-Q.; Kracher, A.; Hannahs, S. T.; Bud'ko, S. L.; Canfield, P. C. *Phys. Rev. B* **2008**, *78*, No. 214515.
(32) Rotter, M.; Pangerl, M.; Tegel, M.; Johrendt, D. *Angew. Chem., Int. Ed.* **2008**, *47*, 7949.
(33) Liu, C.; Palczewski, A. D.; Dhaka, R. S.; Kondo, T.; Fernandes, R. M.; Mun, E. D.; Hodovanets, H.; Thaler, A. N.; Schmalian, J.; Bud'ko, S. L.; Canfield, P. C.; Kaminski, A. *Phys. Rev. B* **2011**, *84*, No. 020509.
(34) Yoshida, T.; Nishi, I.; Ideta, S.; Fujimori, A.; Kubota, M.; Ono, K.; Kasahara, S.; Shibauchi, T.; Terashima, T.; Matsuda, Y.; Ikeda, H.; Arita, R. *Phys. Rev. Lett.* **2011**, *106*, No. 117001.
(35) For example, see: (a) Yin, Z. P.; Haule, K.; Kotliar, G. *Nat. Phys.* **2011**, *7*, 294. (b) Sugimoto, K.; Kaneshita, E.; Tohyama, T. *J. Phys. Soc. Jpn.* **2011**, *80*, No. 033706.
(36) Ishida, S.; Nakajima, M.; Liang, T.; Kihou, K.; Lee, C. H.; Iyo, A.; Eisaki, H.; Kakeshita, T.; Tomioka, Y.; Ito, T.; Uchida, S. 2012, arXiv:1208.1575. arXiv.org e-Print archive. http://arxiv.org/abs/1208.1575.
(37) Allan, M. P.; Chuang, T.-M.; Massee, F.; Xie, Y.; Ni, N; Bud'ko, S. L.; Boebinger, G. S.; Wang, Q.; Dessau, D. S.; Canfield, P. C.; Golden, M. S.; Davis, J. C. 2012, arXiv:1211.6454. arXiv.org e-Print archive. http://arxiv.org/abs/1211.6454.
(38) Ying, J. J.; Wang, X. F.; Wu, T.; Xiang, Z. J.; Liu, R. H.; Yan, Y. J.; Wang, A. F.; Zhang, M.; Ye, G. J.; Cheng, P.; Hu, J. P.; Chen, X. H. *Phys. Rev. Lett.* **2011**, *107*, No. 067001.
(39) Fernandes, R. M.; Abrahams, E.; Schmalian, J. *Phys. Rev. Lett.* **2011**, *107*, No. 217002.
(40) Blomberg, E. C.; Tanatar, M. A.; Fernandes, R. M.; Shen, B.; Wen, H.-H.; Schmalian, J.; Prozorov, R. 2012, arXiv:1202.4430. arXiv.org e-Print archive. http://arxiv.org/abs/1202.4430.
(41) Nakajima, M.; Uchida, S.; Kihou, K.; Lee, C. H.; Iyo, A.; Eisaki, H. *J. Phys. Soc. Jpn.* **2012**, *81*, No. 104710.
(42) Kihou, K.; Saito, T.; Ishida, S.; Nakajima, M.; Tomioka, Y.; Fukazawa, H.; Kohori, Y.; Ito, T.; Uchida, S.; Iyo, A.; Lee, C. H.; Eisaki, H. *J. Phys. Soc. Jpn.* **2010**, *79*, No. 124713.
(43) Rotundu, C. R.; Freelon, B.; Forrest, T. R.; Wilson, S. D.; Valdivia, P. N.; Pinuellas, G.; Kim, A.; Kim, J.-W.; Islam, Z.; Bourret-Courchesne, E.; Phillips, N. E.; Birgeneau, R. J. *Phys. Rev. B* **2010**, *82*, No. 144525.
(44) Liang, T.; Nakajima, M.; Kihou, K.; Tomioka, Y.; Ito, T.; Lee, C. H.; Kito, H.; Iyo, A.; Eisaki, H.; Kakeshita, T.; Uchida, S. *J. Phys. Chem. Solids* **2011**, *72*, 418.
(45) Montgomery, H. C. *J. Appl. Phys.* **1971**, *42*, 2971.